CARBON 48 (2010) 3559–3569

available at www.sciencedirect.com

ScienceDirect

journal homepage: www.elsevier.com/locate/carbon

Surfactant-free dielectrophoretic deposition of multi-walled carbon nanotubes with tunable deposition density

Jason Moscatello, Vijaya Kayastha, Benjamin Ulmen, Archana Pandey, Shun Wu, Abhay Singh, Yoke Khin Yap *

Department of Physics, Michigan Technological University, 118 Fisher Hall, 1400 Townsend Drive, Houghton, MI 49931, USA

ARTICLE INFO

Article history:
Received 16 March 2010
Accepted 25 May 2010
Available online 1 June 2010

ABSTRACT

The effects of AC field strength and AC frequency on the density of dielectrophoretically deposited multi-walled carbon nanotubes (MWCNTs) were investigated and explained in terms of existing theory. We show that while both parameters can be used to control deposition density, the experimentally observed frequency trend can not be explained by the theoretical *Clausius–Mossotti* factors. We demonstrate the ability to make surfactant-free dispersions of long, difficult to disperse MWCNTs and use them with dielectrophoresis to make clean, single and few connections between electrodes.

1. Introduction

Precise placement of individual carbon nanotubes (CNTs) between electrodes is vital for practical device applications. The popularity of CNTs arises due to their unique structural and electronic properties which have facilitated a wide array of applications, examples of which include field-effect transistors [1–5], chemical and biological sensors [6,7], scanning probe microscopy tips [8–10] and field emitters [11,12]. However, it is still challenging to place the carbon nanotubes at desired locations within the devices [13–16].

Many techniques have been used to position CNTs, but each has drawbacks. Spin coating, for example, is convenient and simple, but lacks control of position and distribution [5,17]. Direct growth of CNTs requires high temperatures and has the additional disadvantages of poor selectivity and non-compatibility [18–20]. Manual attachment allows precise placement, but is unviable for devices of any significant density due to the enormous amounts of time necessary to place individual CNTs [21]. Dielectrophoresis (DEP), on the other hand, is quick, convenient, and can result in well-aligned CNTs in the position of interest.

It is well known that single-walled CNTs can be semi-conducting or semi-metallic depending on their structural properties. As the current technology is unable to precisely synthesize single-walled CNTs with desired properties, large-scale application of the semi-metallic multi-walled CNTs (MWCNTs) will definitely come ahead of applications that require semi-conducting CNTs. In particular, MWCNTs are ideal for use as nanowires and nanoelectrodes in devices [22–24]. As DEP was originally applied to dielectric particles, the theoretical principles of DEP are not thoroughly understood for the MWCNTs that have high aspect ratios and are semi-metallic. Thus, it is important to examine the relation between the theory of DEP and its experimental application to deposit MWCNTs between pairs of electrodes.

In this report we focus on two main aspects of the DEP process of MWCNT deposition: (1) controlling the density of MWCNTs across electrode pairs, and (2) depositing unbundled MWCNTs across a pair of electrodes without using surfactants. Although the DEP theory is relatively well established for dielectric particles, for experiments in which MWCNTs are used to span gaps between electrodes, the assumptions of the theory are explicitly violated. We examine

* *Corresponding author:* Fax: +1 906 487 2933.
E-mail address: ykyap@mtu.edu (Y.K. Yap).
0008-6223/$ - see front matter
doi:10.1016/j.carbon.2010.05.054

whether or not the qualitative predictions of the theory continue to give insight into the experimental results in these cases. In addition, of extreme importance to any of these placement techniques is the ability to create suspensions of MWCNTs in liquids, which is difficult due to their generally low solubility and tendency to aggregate. Though surfactants can be used to greatly ease the difficulty of MWCNT dispersion, many applications, such as molecular electronics and (bio)chemical sensors, demand as little contamination as possible. It is necessary, therefore, to develop a method by which to achieve MWCNT suspensions without the use of surfactants. Here we report our method for successful dielectrophoretic deposition of MWCNTs with tunable density, by using surfactant-free dispersions.

2. Dielectrophoretic theory

Whenever a polarizable object is placed within an electric field, charge migration is induced on the material causing a dipole moment with a net positive charge on one side and an a net negative charge on the reverse side. The electric field will act to pull the positive charge in one direction and the negative charge in the reverse direction. In the case of a uniform electric field, these two forces are balanced and the object experiences no net force. However, if the field is non-uniform, the forces will be out of balance and the object will experience a net force [25] – using this force imbalance to deposit material in a desired location is the basis of dielectrophoresis.

2.1. The dipole approximation

If we assume that the presence of the dipole does not alter the field and that the length of the dipole is much less than the characteristic dimension of the field uniformity (the dipole approximation – **Assumption 1**), we can drop higher order terms and arrive at the familiar expressions for a dipole in an electric field [25,26]:

$$\vec{p} = q\vec{d} \tag{1}$$

$$\vec{F}_{\text{dipole}} = \vec{F}_d = q(\vec{d}\cdot\vec{\nabla})\vec{E}(\vec{r}) = (\vec{p}\cdot\vec{\nabla})\vec{E}(\vec{r}) \tag{2}$$

where $\vec{p}$ is the dipole, $\vec{d}$ is the vector describing the separation of the charges of magnitude q in the dipole (pointing from negative to positive charge), $\vec{E}$ is the electric field and $\vec{F}$ is the force the dipole experiences due to the applied electric field. What is immediately apparent is that the theory predicts that only an electric field gradient results in a net force on the dipole. Further, since strength of the induced dipole is proportional to the strength of the externally applied electric field, the force is a function of ∇E^2 and, therefore, is independent of field direction and can be driven by either DC or AC fields [27].

2.2. The Rayleigh electrostatic and the uniform internal field approximations

A more complicated model is necessary to consider non-point objects, like CNTs, in a medium. The common approach is to model the CNTs as slender prolate ellipsoids and to use the Rayleigh electrostatics approximation [28]; the key assumptions are that the CNTs are small compared to the spatial change of the electric field, $|\nabla\vec{E}| \gg l_{cnt}|\nabla\nabla\vec{E}|$, where l_{cnt} is the length of the CNT (**Assumption 2**), and that the induced field internal to the CNTs is uniform (**Assumption 3**) [27]. Then the magnitude of the dipole moment of the CNT can be determined using [26–28]:

$$p_{cnt} = V_{cnt}\varepsilon_m\vec{E}\cdot\vec{P} \tag{3}$$

where V_{cnt} is the volume of the CNT, ε_m is the permittivity of the medium, $\vec{P} = \mathrm{Re}[K^{\parallel}]\vec{u}\vec{u} + \mathrm{Re}[K^{\perp}]\left(\vec{I} - \vec{u}\vec{u}\right)$ is the polarizability tensor, $\vec{u}$ is the unit vector along the CNT axis, $\vec{I}$ is the identity tensor, and Re $[K^{\parallel,\perp}]$ are the real parts of the axial (or parallel) and radial (or perpendicular) Clausius–Mossotti (CM) factors [27]. The CM factors depend on the differences between the complex permittivities of particle material (CNTs) and the medium, and are given for prolate ellipsoids by [27]:

$$K^{\parallel,\perp} = \frac{\varepsilon^*_{cnt} - \varepsilon^*_m}{\varepsilon^*_m + \left(\varepsilon^*_{cnt} - \varepsilon^*_m\right)L^{\parallel,\perp}} \tag{4}$$

where $L^{\parallel,\perp}$ are depolarization factors dependent on geometry. Since CNTs are modeled geometrically to be prolate ellipsoids with high aspect ratios, for this case the depolarization factors are written as [26]:

$$L^{\parallel} = \frac{4r^2_{cnt}}{l^2_{cnt}}\left(\log\left[\frac{l_{cnt}}{r_{cnt}}\right] - 1\right) \tag{5}$$

$$L^{\perp} = \frac{1 - L^{\parallel}}{2} \tag{6}$$

where r_{cnt} is the CNT radius. As expected, the CNTs are more polarizable along the longer axis of the ellipsoid. It is important that the permittivities of the materials are frequency-dependent in AC fields because the charges must move and dissipate energy; this dependence is written as [27,29]:

$$\varepsilon^*(\omega) = \varepsilon - i\frac{\sigma}{\omega} \tag{7}$$

where $\omega = 2\pi f$ is the angular frequency of the AC field. The CNTs are assumed to be a homogeneous material with the same ε_{cnt} and σ_{cnt} for both CM factors because the anisotropy in the dielectric constants is negligible [27]. Further, ε_{cnt} and σ_{cnt} are treated as being independent of frequency, since the values should only begin to deviate from their DC values in the THz range [30].

The result is the CM factors have frequency dependence in both magnitude and phase. The phase angle represents a lag in the induced dipole relative to the changing external field due to a finite charging time [27]. The build-up and decay time are expressed by the Maxwell–Wagner relaxation time constant [26]:

$$\tau^{\parallel,\perp} = \frac{\left(1 - L^{\parallel,\perp}\right)\varepsilon_m + L^{\parallel,\perp}\varepsilon_{cnt}}{\left(1 - L^{\parallel,\perp}\right)\sigma_m + L^{\parallel,\perp}\sigma_{cnt}} \tag{8}$$

$$\omega_C = \frac{1}{\tau^{\parallel}} \tag{9}$$

Here ω_C represents the critical frequency at which the charge within the medium can no longer keep pace with the switching of the AC field, causing a reduction in the dipole moment; for CNTs, the critical frequency of the axial direc-

tion is what matters. Note that it is possible for the CM factors to be or become negative in certain situations. If conditions are such that the particle is more polarizable than the medium, the CM factors are positive and the DEP force pushes the particle to regions of higher electric fields in a process called positive dielectrophoresis. If the medium is more polarizable, the CM factors are negative and the particle is pushed to the weaker regions of electric field; this is called negative dielectrophoresis [25].

We can consider the time-averaged force on the CNTs as well. The time-averaged force on a tube aligned with the field lines can be given by [29]:

$$\langle F_{DEP}\rangle = \frac{1}{2}\pi r_{cnt}^2 l_{cnt}\varepsilon_m \mathrm{Re}(K^{\|})\nabla \mid E\mid^2 \quad (10)$$

This expression makes explicit that the force the CNT feels should be proportional to the gradient of the field strength and the CM factor and, therefore, has a dependence on frequency which predicts the force will drop off quickly above the critical frequency, ω_C. The idea that the average force is proportional to the CM factor is extremely important and will be returned to later in this report. A diagram of a dipole induced in a prolate ellipsoid by a non-uniform electric field is shown in Fig. 1. The instantaneous force vector on the CNT is shown as $\vec{F}_{DEP} = \vec{F}_+ + \vec{F}_-$, where $\vec{F}_+$ and $\vec{F}_-$ are the instantaneous force vectors between the electrodes and the electrostatic poles on the CNT as shown.

3. Experimental procedure

Dielectrophoretic deposition was performed with two types of electrode geometries, (1) large, flat planar electrodes and (2) long, slender microelectrodes. The planar electrode DEP experiments took used a WAVETEK Sweep Generator model 22 as the AC electric field source; the microelectrode DEP experiments used a Tektronix TM502A as the AC electric field source (sinusoidal). In both cases, the waveform frequency and magnitude were verified by an oscilloscope before using them for DEP, then the generator was connected to two tungsten microprobes used to contact the electrodes. The electric fields were always turned on before the drop of suspension was placed on the gap, and were turned off 5 s after the drop of solution looked completely evaporated under the optical microscope. All experiments were conducted using thermal chemical vapor deposition (T-CVD) and plasma-enhanced chemical vapor deposition (PE-CVD) grown MWCNTs made in-house, the details of which can be found in references [31] and [32], respectively. Briefly, PE-CVD tubes are short with a relatively low aspect ratio (3 μm × 50 nm) while T-CVD grown MWCNTs are longer and thinner (13 μm × 20–30 nm) and, as a result, tend to be tangled and difficult to separate in solution. Because the PE-CVD tubes are easier to disperse, they are tested first, while the T-CVD MWCNTs are to be used in the final devices, but offer a greater challenge due to their tendency to tangle. Results were observed using a Hitachi S4700 field-emission scanning electron microscope (SEM). MWCNT solutions were made by removing the tubes from the growth substrate by scalpel, and placing them in 200 proof ethanol where they undergo ultrasonication.

4. Results and discussion

4.1. Flat electrode gaps

Initial experiments utilized the simple geometry of a flat gap between large planar electrodes for MWCNT deposition. Electrodes were patterned on glass substrates by pulsed laser deposition (PLD) of an iron film to a thickness of 50 nm. The gaps of roughly 1 μm were made by focused ion beam (FIB) milling. MWCNT dispersions were made from MWCNTs grown by the PE-CVD process [32], grown directly on the catalyst-film coated substrates. After growth, the 3.85 mm^2 growth region was removed and placed in ethanol for dispersion to a density of roughly 10^8 MWCNTs per mL. The suspen-

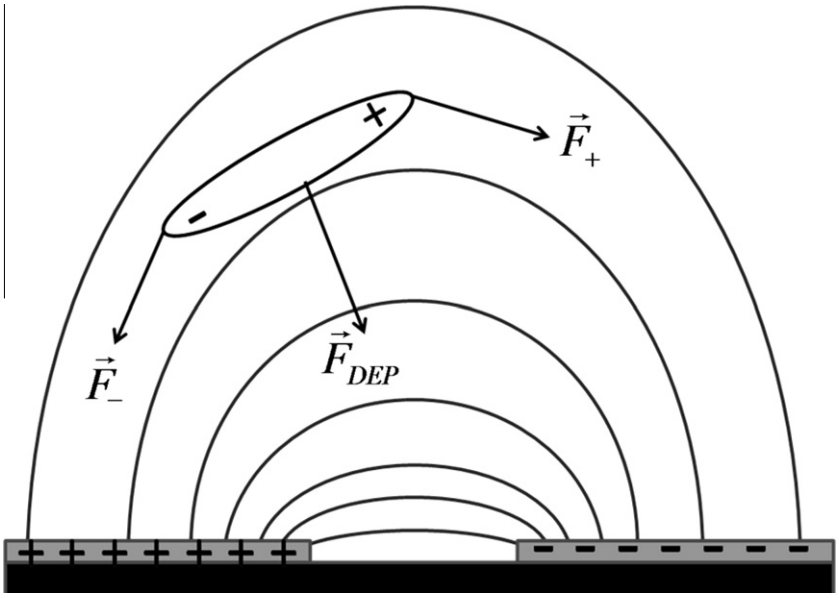

Fig. 1 – A CNT (modeled as a single dipole in a prolate ellipsoid) in the electric field between two charged electrodes.

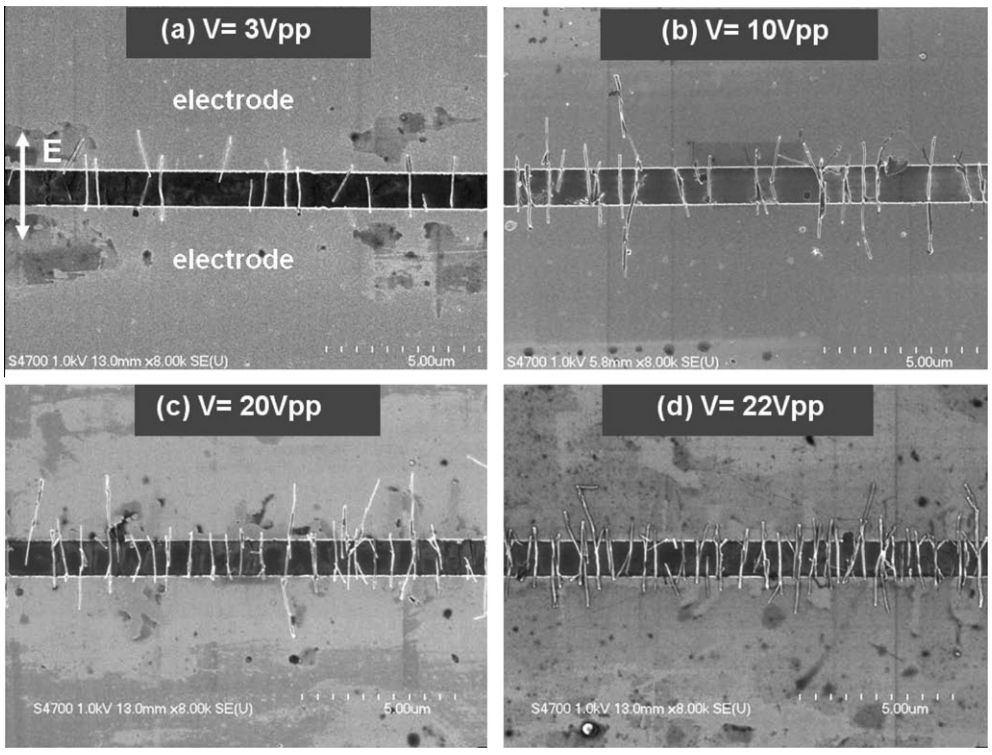

Fig. 2 – MWCNT deposition with varying sinusoidal AC voltage. Frequency was kept fixed at 2 MHz. The density of MWCNTs in the gap increases with increasing applied voltage.

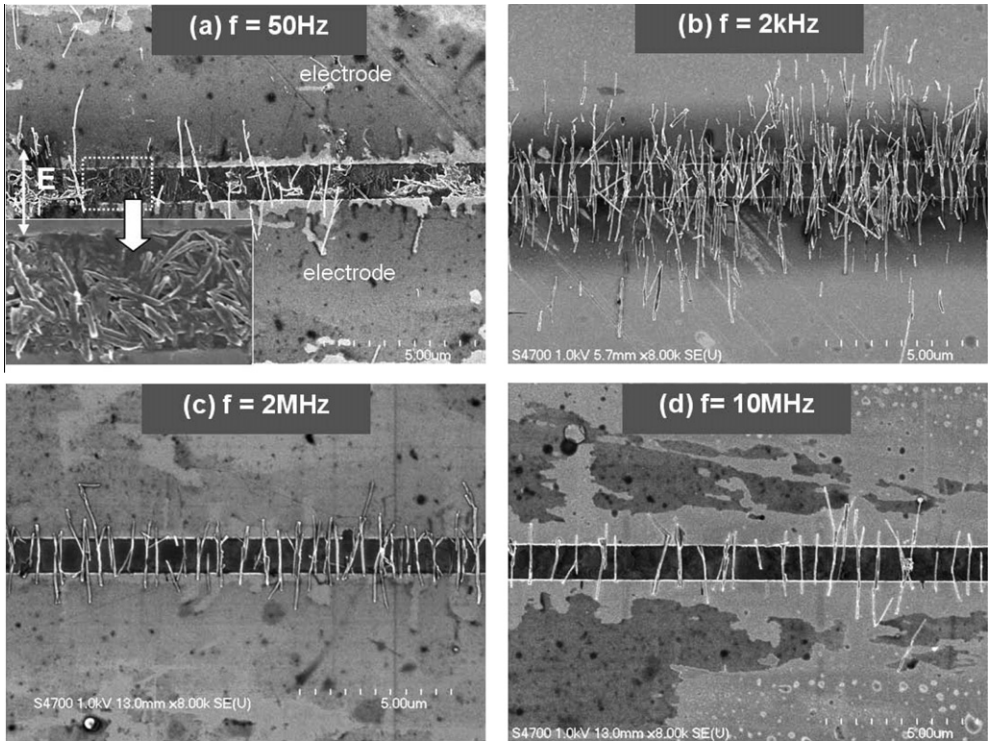

Fig. 3 – MWCNT deposition with varying sinusoidal AC frequency. Voltage was kept fixed at 20 V_{pp}. (a) At low frequency (50 Hz) the deposition is sporadic and contains a high level of impurities in the gap region (inset). (b to d) Density of deposited tubes peaks at 2 kHz, then decreases with increasing frequency through 10 MHz; there are little to no impurities deposited in the region of interest.

sion was placed in an ultrasonication bath for 2 h to facilitate dispersion.

Deposition was performed by turning on the AC field and applying a 40 μL drop of the ethanol/MWCNT dispersion directly to the gap, giving it time to completely dry before the applied field is turned off. In order to observe the effect of applied field strength, the frequency was fixed to 2 MHz while varying the voltage from 3 to 22 V_{pp}; Fig. 2 shows the results of this test. Clearly the density (number of MWCNTs per unit length of the electrode gap) of tubes increases along with increasing field strength. Alignment is generally good with no apparent dependence on the field strength. Field strength is, therefore, one method of controlling the spacing between MWCNTs, which is important for the fabrication of density-dependent parallel nanoelectronic devices.

Next, the voltage was held at 20 V_{pp} and the frequency varied in order to study the effects of AC frequency on DEP; the results are shown in Fig. 3. Low frequencies (a) 50 Hz showed the MWCNTs clumping on the gap with little to no alignment. Increasing the field to higher frequencies (b) 2 kHz and (c) 2 MHz showed increased alignment and higher density than the clumps seen at 50 Hz. At (d) 10 MHz, the MWCNTs show alignment, but a remarkably lower density; the bundles of tubes are farther apart and contain fewer tubes per bundle. This shows that the degree of alignment and MWCNT density can be tuned by controlling the AC frequency of the applied field.

All results were reproduced and confirmed by DEP with CNTs grown by T-CVD processes as well. For example, the tendency of the MWCNT density to decrease once the AC frequency has passed a critical frequency is shown in Fig. 4 for thermally grown MWCNTs (with a gap of ~40 μm). Here a 20 V_{pp} field was used and clearly shows better alignment and lower density at 5 MHz than 3 MHz. As the gap is bigger than the length of these CNTs, once a tube touches an electrode, it acquires the potential of the electrode and can attract other MWCNTs to itself, leading to the chains observed by the SEM.

One aspect of the results is simple to determine: since higher electric fields result in higher field-induced forces on the CNTs, higher electric field yields a higher density of oriented tubes. The MWCNTs feel more force and are able to reach the deposition region before the solution evaporates. However, from the data it is clear that deposited MWCNT density rises, peaks and falls with increasing frequency, which is not as straightforward to understand. Going back to the theory, we must look to the CM factor, proportional to the time-averaged force, which indicates the there *should* be a fall as frequency increases beyond ω_C. This happens because the response of the electrons in the MWCNTs can no longer keep pace with the oscillating AC field and as a result the maximum induced dipole moment shrinks. Smaller induced dipole means lower force, so the MWCNTs do not have enough time before solution evaporation to reach the gap in the numbers they could below the critical frequency. However, the CM factor cannot explain why at low frequency the CNTs are present in lower numbers.

We believe the poor alignment and low density of deposited MWCNTs is best explained by the formation of an electrical double-layer forming near the electrode surfaces. Trace impurities exist in the ethanol, and others may have been

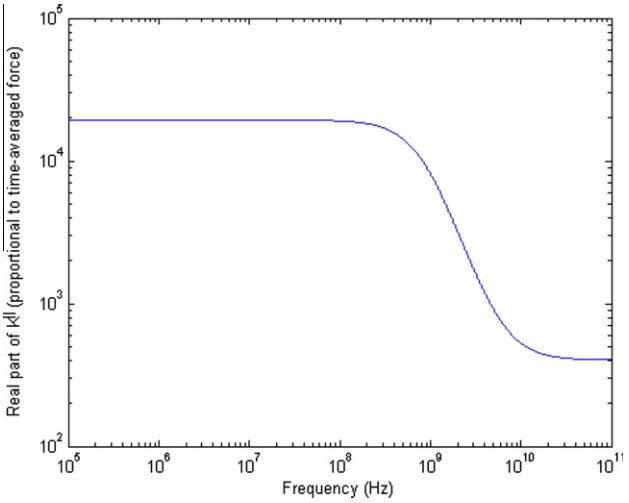

Fig. 5 – Plot of the real part of the CM factor for CNTs of the aspect ratio of the in-house T-CVD MWCNTs. The CM factor predicts no perceptible drop in time-averaged dipole force over the frequencies investigated, in contrast with experimental results.

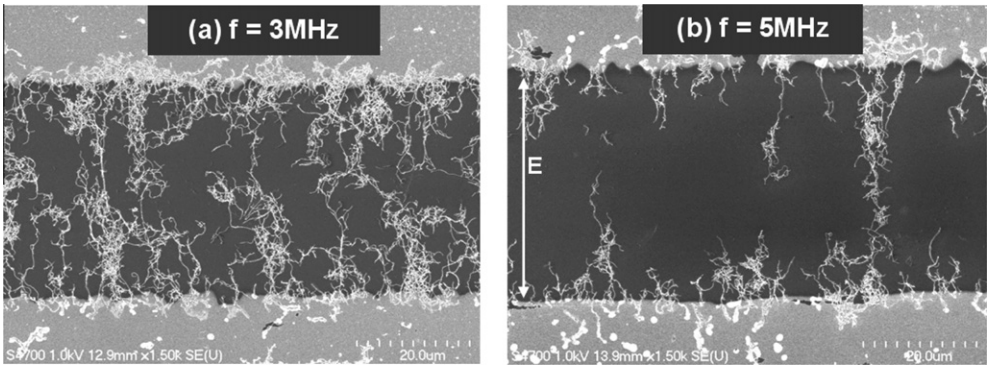

Fig. 4 – Effect of varying the frequency on thermal-CVD grown MWCNTs. The T-CVD tubes experience the same trend of decreasing density with increasing field strength as the PE-CVD tubes.

incorporated into the ethanol during the sonication process, though not to the extent that would inhibit the DEP mechanism. As a voltage is applied, these trace ions and molecules with induced dipoles move to the surface of the electrode. Specifically adsorbed particles form what is referred to as the inner Helmholtz plane on the surface [33]. Beyond the inner Helmholtz plane is a layer of diffuse attracted molecules called the outer Helmholtz plane [33]. If a double-layer is given time to form, it can screen nearly all of the applied voltage [33–35]. However, formation of the double-layer takes time – the effect we see is due to this finite charging time. When the switching of electrode polarity is very slow, such as in the 50 Hz range, the double-layer has time to form and greatly screens the electric potential. As the AC frequency increases, the double-layer becomes less and less well formed until we reach a frequency beyond which it has insufficient time to form and no longer screens the electric field [33–35]; from this point on the effect of the CM factor dominates MWCNT deposition density.

One last observed frequency-dependent phenomenon is that of contamination. At 50 Hz, Fig. 3(a, inset), it is clear there are large amounts of impurities gathered in the gap and coating the MWCNTs, but this effect is notably absent at higher frequencies. The answer to this goes back to the CM factors for the contaminant particles. The MWCNTs always have positive CM factors because their semi-metallic nature makes them much more polarizable than the solvent (ethanol) they are deposited in. This is not necessarily true for contami-

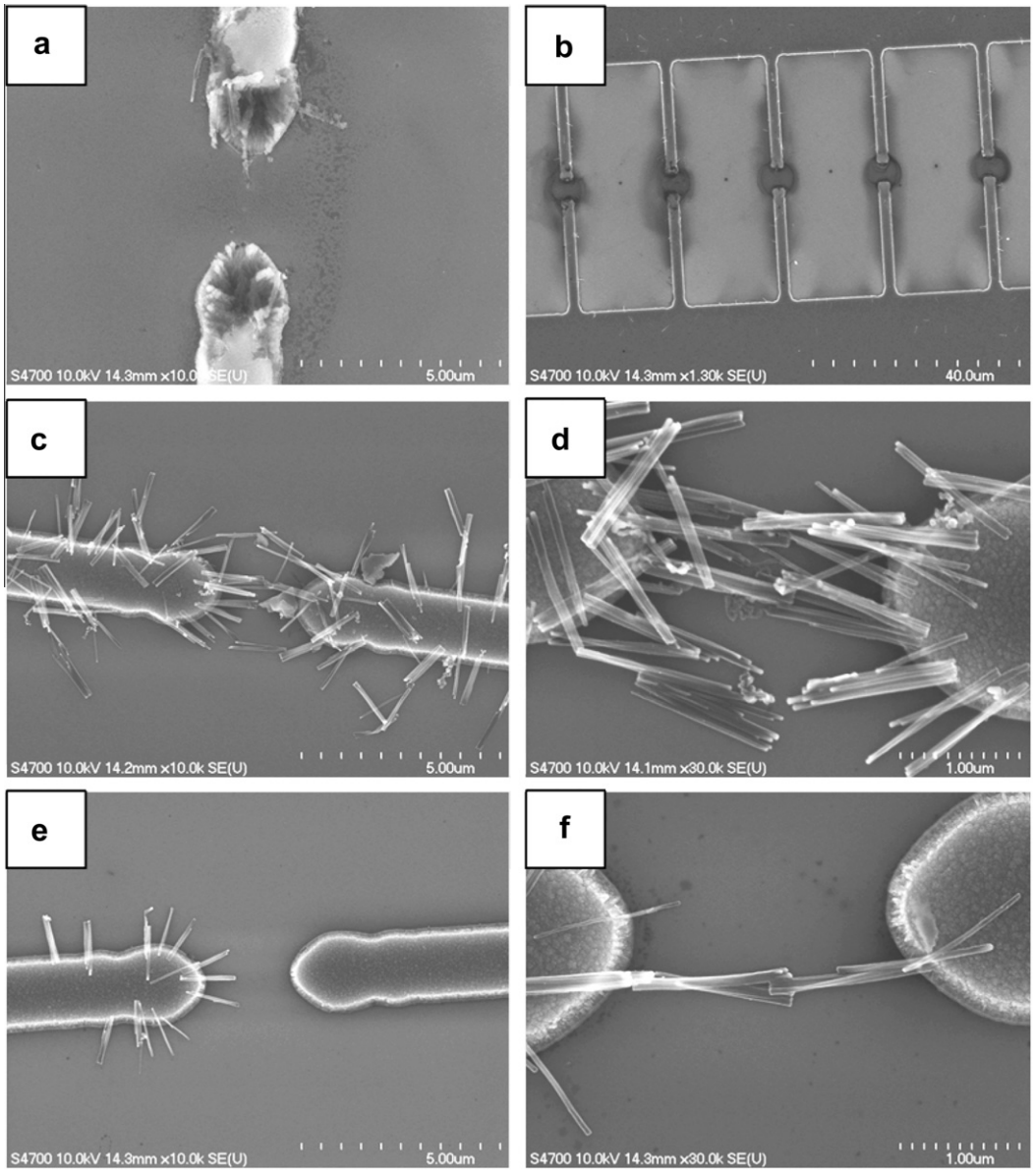

Fig. 6 – Effect of frequency for dielectrophoretic deposition of PE-CVD grown MWCNTs without surfactants. Voltage was held at 30 V_{pp}. (a and b) Deposition at 50 Hz shows little deposition and a very localized accumulation of impurities. (c and d) Deposition at 2 kHz is extremely dense with no impurities in the region of interest. (e and f) Deposition at 2 MHz is significantly less than at 2 kHz.

nants, some of which can be more polarized than the solvent at low frequency, but as frequency increases can quickly pass their critical frequency and become less polarized than the solution, beginning to experience negative dielectrophoresis. Therefore, at higher frequencies the impurities move to the areas of lowest field strength, leaving the areas of interest clean. Apparently the detected impurities have higher dielectric properties than the MWCNTs and are likely amorphous particles.

4.2. *Clausius–Mossotti factor predictions*

So far the CM factor has been discussed qualitatively in terms of how it relates to the results of the deposition – but how does it compare quantitatively? A calculation for the CM factor of our MWCNTs was carried out using the following values: $\varepsilon_{cnt} = 8.854 \times 10^{-8}$ F/m [36], $\varepsilon_{ethanol} = 2.1516 \times 10^{-10}$ F/m [37], $\sigma_{cnt} = 2.221 \times 10^{4}$ S/m [38] and $\sigma_{ethanol} = 1.3. \times 10^{-7}$ S/m [39] with dimensions equal to the T-CVD grown MWCNTs, $r = 0.02$ μm and $l = 13$ μm. Fig. 5 shows the resulting predictions of the CM model, which indicate the time-averaged force, should be roughly constant over the frequencies investigated. In fact, the critical frequency predicted is $f \approx 5 \times 10^{9}$ Hz, well above the observed frequencies over which force (and density) begin to fall (for $l = 2$ μm, the critical frequency prediction is still on the order of 10^{9} Hz).

That the theory does not match our observation is not surprising. Since in our experiments the MWCNTs are meant to lay entirely across the electrode gaps, all three numbered assumptions mentioned earlier are violated, including the assumption that there is only a single dipole. Therefore, the theory that depends on them cannot accurately apply to the experiments we carry out. In addition, it has also been reported that the situation is far more complex than the theory currently accounts for. For example, the substrate plays a role in dielectrophoresis and, for surfactant–free deposition as conducted here, the solvated molecules affect the dielectric permittivity of the MWCNTs [40], so we know the model is not sufficiently complete. However, the basic trend predicted and explained by the CM factor is still present. We observe that density of deposited MWCNTs decreases with increasing frequency, only the threshold has changed. Voltage can be relied upon to modulate density since the effect is straightforward. In short, we have experimentally determined that DEP force (CM factor) will reduce at the frequency range of MHz, which is lower that the predicted GHz range. Yet knowing that the situation is more complex than our ability to predict, the question remains: will we be able to tune the density of deposited MWCNTs within the same frequency range when the geometry is changed from simple planar electrodes to more geometrically complex microelectrode fingers?

4.3. *Microelectrode fingers*

The next goal was to see if we could extend the frequency dependence result to small gaps (about 2 μm) that are not long channels as before, but between arrays of thin "fingers." The microelectrode fingers are 250 nm thick Ni films patterned using photolithography techniques coupled with plasma sputtering; the substrate is *p*-type silicon with a 120 nm SiO_2 layer. Initial MWCNT solutions were made using the PE-CVD grown tubes. The entire 3.85 mm^2 growth area was dispersed into 50 mL of ethanol by immersing the growth substrate into the solution during ultrasonication. The ultrasonicating bath was continued for 2 h to facilitate unbundling of the MWCNTs, though the tubes are still partially bundled. Before DEP, the solution was re-sonicated for 30 s before each deposition. A wave generator and a microprobe station completed the external circuit, starting the AC field before the introducing the solution. A 10 μL biological syringe was used to place a roughly 5 μL drop of the MWCNT-ethanol solution directly on the pattern and allowed to dry before the AC field was turned off.

Fig. 6 shows the representative results for varying the electric field from (a–b) 50 Hz to (c–d) 2 kHz to (e–f) 2 MHz with 30 V_{pp} applied. Fig. 6(b) shows that for very low field frequencies almost no MWCNTs are deposited preferentially to the gap. However, a short range deposition of contamination can be seen. At such low frequency the impurity particles experience positive DEP, but the electrical double-layer keeps the force relatively weak and therefore results in only local contamination. The double-layer is responsible for the lack of MWCNT deposition as well; this is consistent with our previous results for the flat electrode gap. In Fig. 6(d) it is clear that 2 kHz shows a massive deposition of MWCNTs making parallel connections between the fingers. Fig. 6(f) demon-

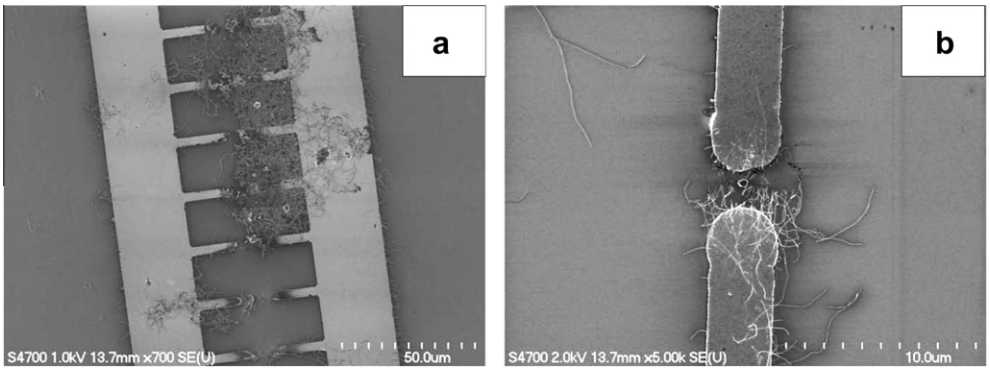

Fig. 7 – (a) Below 2.75 h of sonication, the MWCNTs remain in large tangles. (b) At 3.5 h and above the majority of tubes are broken into fragments too small to span the gap.

strates that there is still a critical frequency above which the DEP force falls off quickly. This means the critical frequency is still well within our frequency range, even with the new geometry. We can, therefore, use frequency as a tool to tune the amount of deposition between the microelectrode fingers.

4.4. *Surfactant-free deposition of T-CVD MWCNTs*

While we have demonstrated the tunability of deposited MWCNTs by voltage and frequency, the PE-CVD tubes were too short for the 2 μm gap and were still clumped. Further work has resulted in the ability to reach our goal of surfactant-free deposition of MWCNTs spanning the gap entirely, and performed using T-CVD grown MWCNTs. In order to do this, a method had to be found to disperse the long, flexible and difficult to disentangle MWCNTs. Most reported work discussed the issue of dispersion in minimal detail [41–43].

Our investigation has shown there is a small window for which T-CVD grown MWCNTs in ethanol can be well dispersed without surfactants and without prohibitive amounts of breakage. A growth region of ~16 mm^2 is put into 20 mL of 200 proof ethanol to form the solution; the MWCNT concentration is estimated to be 0.56 mg/mL. Ultrasonication using a Sonics Vibra-Cell ultrasonicator for 3 h at 80% amplitude results in the desired solution. The quality dispersion window is about 45 min wide, below 2.75 h the tubes are still very tangled and clumped, and at 3.5 h and above the tubes have broken too much into smaller pieces, hindering their ability to span the gap. Examples of under- and over-sonicated are shown in Fig. 7(a) and (b), respectively. As shown in Fig. 7(b), some longer CNTs were occasionally deposited beyond the gap region, which may be avoided by centrifuge the nanotubes suspension.

It appears the dispersion is a two-step process. First is the untangling in which smaller bundles of tubes are freed from

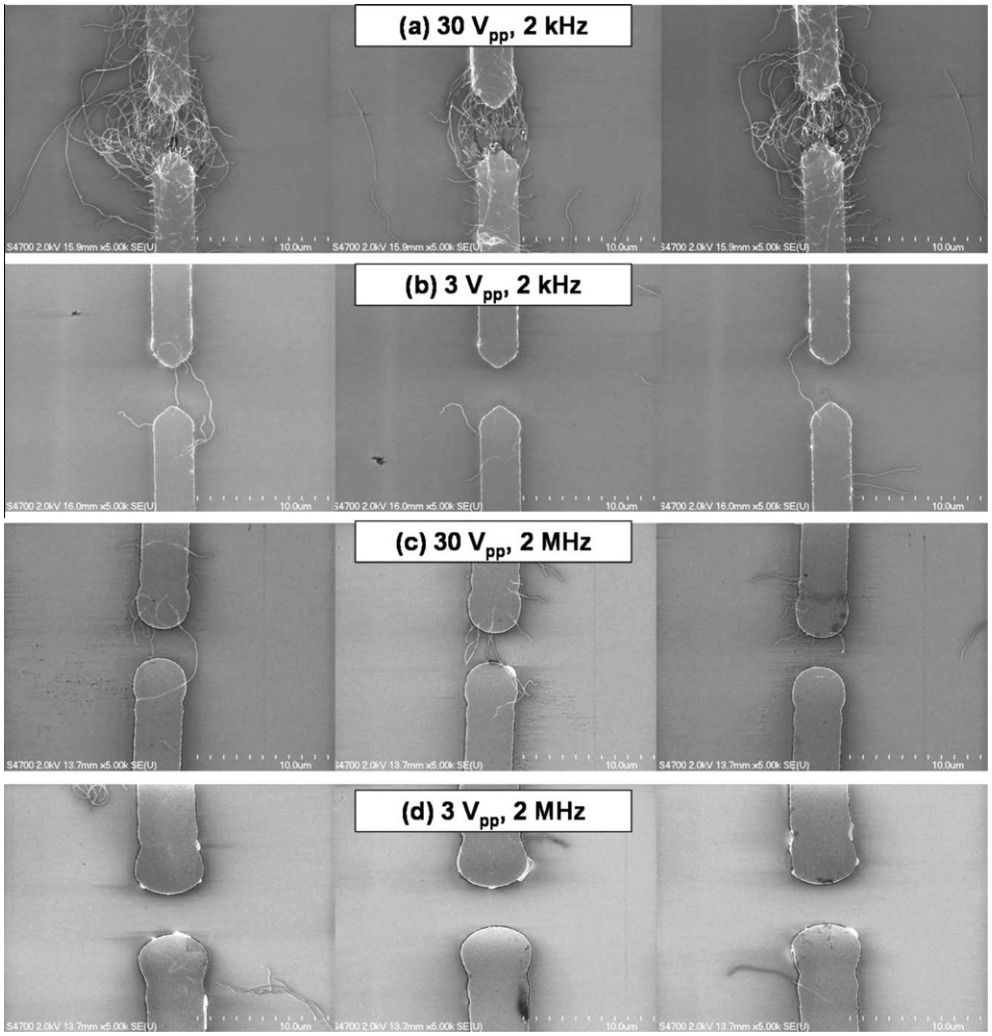

Fig. 8 – Representative SEM micrographs of dielectrophoretic deposition of T-CVD grown MWCNTs without the aid of surfactants showing the effects of field strength and frequency. Optimum deposition takes place at (a) 30 V_{pp} at 2 kHz. By either lowering the field strength to (b) 3 V_{pp} or raising the frequency to (c) 2 MHz, the deposition results in most gaps exhibiting single or few MWCNT connections. If the frequency is raised to 2 MHz and the voltage dropped to 3 V_{pp} simultaneously (d), the deposition has been reduced to none.

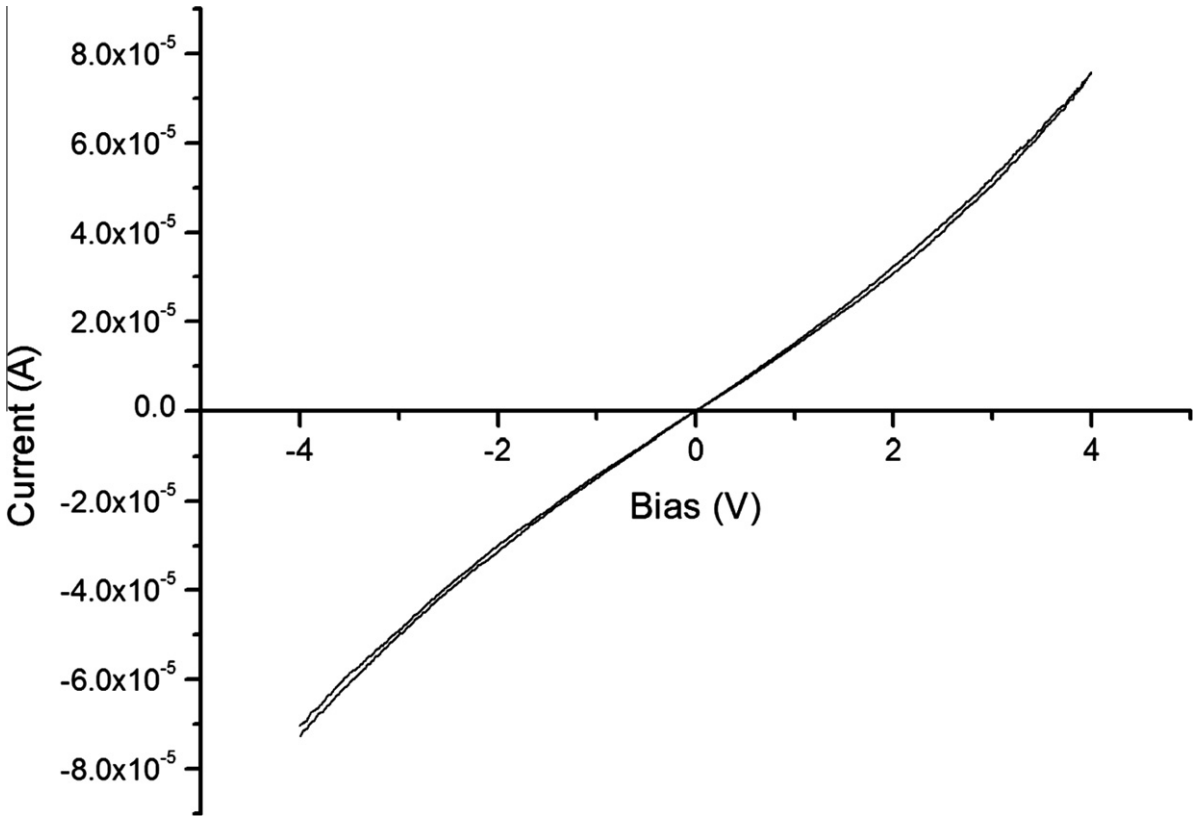

Fig. 9 – Current–voltage characteristics of thermal-CVD grown MWCNTs deposited between 20 and 40 nm Cr/Au nanoelectrode fingers at 30 V_{pp}, 2 kHz.

the greater tangle of MWCNTs, after which begins the unbundling. Because the tubes in large tangles are not as free to vibrate, they do not break even over several hours of ultrasonication time, until they have untangled. The subsequent unbundling process appears to take place much more quickly. Previous experiments indicate that if the MWCNT density in the solution is not low enough, there will never be a phase in which the majority of tubes are untangled and unbroken.

Two things must be noted. First, the optimal ultrasonication time is entirely dependent on the density of the solution – longer times are necessary for higher densities, though there seems to be a maximum density above which good unbroken dispersions are impossible. Second, the solution must never be allowed to rest. Once ultrasonication stops, the tubes immediately begin to re-aggregate, so they must be used immediately. Solutions must be made fresh or resonicating the solution will result in over-sonication and a large percentage of broken tubes.

This dispersion technique was used to prepare a solution for dielectrophoretic deposition of T-CVD MWCNTs, the results of which are shown in Fig. 8; frequencies of 50 Hz were not repeated because they are undesirable for use. Maximum deposition takes place at (a) 30 V_{pp} at 2 kHz. By either lowering the field strength to (b) 3 V_{pp} or raising the frequency to (c) 2 MHz, the deposition is tuned such that most gaps contain single or few MWCNT connections between electrodes, though ~10% do not have a connection. Preliminary data suggests that for those that do have connections, roughly 1/3 are single connections and the remaining 2/3 are few (2–4) connections. If the frequency is raised to 2 MHz and the voltage dropped to 3 V_{pp} simultaneously (d), the deposition has been reduced to none. It should be noted that we have found that the same tunability is not limited to Ni electrode systems, but can be demonstrated using dual-layer Cr/Au electrodes; example I–V characteristics of thermal-CVD MWCNTs deposited in this manner are shown in Fig. 9. The resistance of the deposited MWCNTs is estimated as ~0.60 MΩ by assuming a linear I–V relation.

Finally, we have reached our desired result of clean, surfactant-free deposition of MWCNTs connecting electrodes with density tunable by two parameters: AC field strength and AC field frequency. We believe that our result will be useful for future application of MWCNTs in devices that require minimal contamination.

5. Summary

Though the formalism used to derive the CM factors contain several assumption that are explicitly violated by the goals of placing MWCNTs across gaps between electrodes, it has been shown that their qualitative predictions still hold – frequency, as well as field strength, can be used to tune the density of deposited MWCNTs. Experimentally, we found that the density of dielectrophoretically deposited MWCNTs drops dramatically as the frequency moves from 2 kHz to 2 MHz for

both planar electrode gaps and microelectrode finger gaps. This frequency range is much lower than the critical frequency ($f \approx 5 \times 10^9$ Hz) predicted by the CM factors. Further, we have demonstrated T-CVD grown MWCNTs, extremely difficult to disperse, *can* be dispersed into ethanol without the aid of surfactants *via* a small window after 3 h of ultrasonication that untangles and unbundles the MWCNTs, but leaves them long enough to span the electrode gaps. Combining these techniques allows clean, surfactant-free MWCNT connections of controllable density between electrodes.

Acknowledgements

This work is supported by Defense Advanced Research Projects Agency (Contract No.: DAAD17-03-C-0115, through Army Research Laboratory). We thank Professor Craig Friedrich of the Multi-Scale Technologies Institute (*MuSTI*), and Professor Jacek Borysow of the Department of Physics at Michigan Technological University for their support.

REFERENCES

[1] Li H, Zhang Q, Li J. Carbon-nanotune-based single-electron/hole transistors. Appl Phys Lett 2006;88(1):013508/1–3.
[2] Javey A, Guo J, Farmer DB, Wang Q, Wang D, Gordon RG, et al. Carbon nanotube field-effect transistors with integrated ohmic contacts and high-κ gate dielectrics. Nano Lett 2004;4(3):447–50.
[3] Martel R, Schmidt T, Shea HR, Hertel T, Avourisa Ph. Single- and multi-wall carbon nanotube field-effect transistors. Appl Phys Lett 1998;73(17):2447–9.
[4] Wind SJ, Appenzeller J, Martel R, Derycke V, Avourisa Ph. Vertical scaling of carbon nanotube field-effect transistors using top gate electrodes. Appl Phys Lett 2002;80(20):3817–9.
[5] Tans SJ, Verschueren ARM, Dekker C. Room-temperature transistor based on a single carbon nanotube. Nature 1998;393:49–52.
[6] Kong J, Franklin NR, Zhou C, Chapline MG, Peng S, Cho K, et al. Nanotube molecular wires as chemical sensors. Science 2000;287(5453):622–5.
[7] Collins PG, Bradley K, Ishigami M, Zettl A. Extreme oxygen sensitivity of electronic properties of carbon nanotubes. Science 2000;287:1801–4.
[8] Dai H, Hafner JH, Rinzler AG, Colbert DT, Smalley RE. Nanotubes as nanoprobes in scanning probe microscopy. Nature 1996;384:147–50.
[9] Snow ES, Campbell PM, Novak JP. Single-wall carbon nanotube atomic force microscope probes. Appl Phys Lett 2002;80(11):2002–4.
[10] Hafner JH, Cheung CL, Lieber CM. Growth of nanotubes for probe microscopy tips. Nature 1999;398:761–2.
[11] Ulmen B, Kayastha VK, DeConinck A, Wang J, Yap YK. Stability of field emission current from various types of carbon nanotube films. Diamond Relat Mater 2006;15(2–3):212–6.
[12] Pandey A, Prasad A, Moscatello J, Ulmen B, Yap YK. Enhanced field emission stability and density produced by conical bundles of catalyst-free carbon nanotubes. Carbon 2010;48(1):287–92.
[13] Ding D, Chen Z, Rajaputra S, Singh V. Hydrogen sensors based on aligned carbon nanotubes in an anodic aluminum oxide template with palladium as a top electrode. Sens Actuators B 2007;124(1):12–7.
[14] Fennimore AM, Yuzvinsky TD, Han WQ, Fuhrer MS, Cumings J, Zettl A. Rotational actuators based on carbon nanotubes. Nature 2003;424:408–10.
[15] Baughman RH, Cui C, Zakhidov AA, Iqbal Z, Barisci JN, Spinks GM, et al. Carbon nanotube actuators. Science 1999;284(5418):1340–4.
[16] Hall AR, Falvo MR, Superfine R, Washburn SA. A self-sensing nanomechanical resonator built on a single-walled carbon nanotube. Nano Lett 2008;8(11):3746–9.
[17] Bachtold A, Hadley P, Nakanishi T, Dekker C. Logic circuits with carbon nanotube transistors. Science 2001;294(5545):1317–20.
[18] Javey A, Shim M, Dai H. Electrical properties and devices of large-diameter single-walled carbon nanotubes. Appl Phys Lett 2002;80(6):1064–6.
[19] Liu X, Lee C, Zhou C, Han J. Carbon nanotube field-effect inverters. Appl Phys Lett 2001;79(20):3329–31.
[20] Oh BS, Min YS, Bae EJ, Kang D, Jung IS, Hwang CS, et al. Fabrication of suspended single-walled carbon nanotubes *via* a direct lithographic route. J Mater Chem 2006;16(2):174–8.
[21] Fukuda T, Arai F, Dong L. Assembly of nanodevices with carbon nanotubes through nanorobotic manipulations. Proc IEEE 2003;91(11):1803–18.
[22] Kreupl F, Graham AP, Duesberg GS, Steinhögl W, Liebau M, Unger E, et al. Carbon nanotubes in interconnect applications. Microelectron Eng 2002;64(1–4):399–408.
[23] Lin Y, Lu F, Tu Y, Ren Z. Glucose biosensors based on carbon nanotube nanoelectrode ensembles. Nano Lett 2004;4(2):191–5.
[24] Li J, Ng HT, Cassell A, Fan W, Chen H, Ye Q, et al. Carbon nanotube nanoelectrode array for ultrasensitive DNA detection. Nano Lett 2003;3(5):572–602.
[25] Burke PJ. Nanodielectrophoresis: electronic nanotweezers. In: Nalwa HS, editor. Encyclopedia of nanoscience and nanotechnology, vol. 6. American Scientific Publishers. p. 623–41.
[26] Jones TB. Electromechanics of particles. New York, NY: Cambridge University Press; 1995.
[27] Mendes MJ, Schmidt HK, Pasquali M. Brownian dynamics simulations of single-wall carbon nanotube separation by type using dielectrophoresis. J Phys Chem B 2008;112(25):7467–77.
[28] Bohren CF, Huffman DR. Absorption and scattering of light by small particles. New York, NY: Wiley-VCH; 1983.
[29] Kim J-E, Han C-S. Use of dielectrophoresis in the fabrication of an atomic force microscope tip with a carbon nanotube: a numerical analysis. Nanotechnology 2005;16(10):2245–50.
[30] Ugawa A, Rinzler AG, Tanner DB. Far-infrared gaps in single-wall carbon nanotubes. Phys Rev B (Condens Mater Phys) 1999;60(16):R11305–8.
[31] Kayastha VK, Yap YK, Pan Z, Ivanov IN, Puretzky AA, Geohegan DB. High-density vertically aligned multiwalled carbon nanotubes with tubular structures. Appl Phys Lett 2005;86(25):253105/1–3.
[32] Menda J, Ulmen B, Vanga LK, Kayastha VK, Yap YK, Pan Z, et al. Structural control of vertically aligned multiwalled carbon nanotubes by radio-frequency plasmas. Appl Phys Lett 2005;87(17):173106/1–3.
[33] Bard AJ, Faulkner LR. Electrochemical methods: fundamentals and applications. New York, NY: John Wiley & Sons, Inc.; 2001.
[34] Ramos A, Morgan H, Green NG, Castellanos A. Ac electrokinetics: a review of forces in microelectrode structures. J Phys D Appl Phys 1998;31:2338–53.

[35] Schwan HP. Electrode polarization impedance and measurements in biological materials. Ann NY Acad Sci 1968;148(1):191–209.
[36] Dimaki M, Bøggild P. Dielectrophoresis of carbon nanotubes using microelectrodes: a numerical study. Nanotechnology 2004;15(8):1095–103.
[37] Landolt-Börnstein. Static dielectric constants of pure liquids and binary liquid mixtures: supplement to IV/6. Berlin: Heidelberg, Springer; 2008.
[38] Chan RHM, Fung CKM, Li WJ. Rapid assembly of carbon nanotubes for nanosensing by dielectrophoretic force. Nanotechnology 2004;15(10):S672–7.
[39] Dean JA. Lange's handbook of chemistry. 14th ed. McGraw Hill, Inc.; 1992.
[40] Duchamp M, Lee K, Dwir B, Seo JW, Kapon E, Forró L, et al. Controlled positioning of carbon nanotubes by dielectrophoresis: insights into the solvent and substrate role. ACS Nano 2010;4(1):279–84.
[41] Chen XQ, Saito T, Yamada H, Matsushige K. Aligning single-wall carbon nanotubes with an alternating-current electric field. Appl Phys Lett 2001;78(23):3714–6.
[42] Seo H-W, Han C-S, Choi D-G, Kim K-S, Lee Y-H. Controlled assembly of single SWNTs bundle using dielectrophoresis. Microelectron Eng 2005;81:83–9.
[43] Chung J, Lee K-H, Lee J, Ruoff RS. Toward large-scale integration of carbon nanotubes. Langmuir 2004;20(8):3011–7.